




Inhibition of zDHHC7-driven protein S-palmitoylation prevents cognitive deficits in an experimental model of Alzheimer's disease

Francesca Natale^{a,b,1}, Matteo Spinelli^{a,b,1} , Marco Rinaudo^{a,b} , Walter Gulisano^c, Ida Nifo Sarrapochiello^a , Giuseppe Aceto^a , Daniela Puzzo^{c,d} , Salvatore Fusco^{a,b,2} , and Claudio Grassi^{a,b} 

Affiliations are included on p. 10.

Edited by Ana Maria Cuervo, Albert Einstein College of Medicine, Bronx, NY; received February 8, 2024; accepted October 4, 2024

Protein post-translational modifications (PTM) play a crucial role in the modulation of synaptic function and their alterations are involved in the onset and progression of neurodegenerative disorders. S-palmitoylation is a PTM catalyzed by zinc finger DHHC domain containing (zDHHC) S-acyltransferases that affects both localization and activity of proteins regulating synaptic plasticity and amyloid- β ($A\beta$) metabolism. Here, we found significant increases of both zDHHC7 expression and protein S-palmitoylation in hippocampi of both 3 \times Tg-AD mice and post-mortem Alzheimer's disease (AD) patients. Chronic intranasal administration of the S-palmitoylation inhibitor 2-bromopalmitate counteracted synaptic plasticity and cognitive deficits, reduced the $A\beta$ deposition in the hippocampus and extended the lifespan of both male and female 3 \times Tg-AD mice. Moreover, hippocampal silencing of zDHHC7 prevented the onset of cognitive deficits in the same experimental model. We also identified a FoxO1-mediated epigenetic mechanism inducing zDHHC7 expression, which was triggered by brain insulin resistance in 3 \times Tg-AD mice. Finally, in hippocampi of AD patients S-palmitoylation levels of Beta-Secretase 1 were associated with $A\beta$ 1 to 42 load and they inversely correlated with Mini Mental State Examination scores. Our data reveal a key role of both zDHHC7 overexpression and protein hyperpalmitoylation in the onset and progression of AD-related alterations of synaptic plasticity and memory.

brain insulin resistance | protein S-palmitoylation | BACE1 | Alzheimer's disease | zDHHC

Alzheimer's disease (AD) is a growing health and socioeconomic problem for aging populations worldwide and it represents one of the most demanding challenges for biomedical and pharmacological research (1). Amyloid- β ($A\beta$) deposits and hyperphosphorylated tau aggregates are AD neuropathological hallmarks (2), but the molecular mechanisms underlying the development of the disease are not yet fully known. Alteration of brain insulin signaling has been demonstrated to induce an AD-like phenotype by accelerating neurodegeneration in the hippocampus and neocortex of experimental models of AD (3). We found that aberrant protein S-palmitoylation plays a pivotal role in the brain insulin resistance (BIR)-dependent cognitive decline (4). S-acylation is a protein post-translational modification (PTM) consisting in the covalent attachment of a fatty acid molecule to cysteine residues through the formation of a thioester bond. S-palmitoylation is the most common S-acylation (hereinafter defined S-palmitoylation) occurring inside the cells (5). It influences protein trafficking toward cellular membranes and is finely regulated by a class of enzymes named zinc finger DHHC domain containing (zDHHC) S-acyltransferases (6). An increasing number of studies has shown the role of palmitoylated proteins in the regulation of synaptic plasticity and neuronal functions (7). It has also been reported that proteins critically involved in AD (e.g., the amyloid precursor protein, amyloid precursor protein (APP), and Beta-Secretase 1, BACE1) are targets of S-palmitoylation (8, 9). Alterations of zDHHC expression and function have been theorized to be implicated in the pathogenesis of neurodegenerative diseases (10, 11). However, the role of zDHHC enzymes and protein S-palmitoylation in the onset and progression of neurodegeneration and cognitive deficits in AD remains largely unknown. Here, we reported that 3 \times Tg-AD mice, a well-characterized experimental model of AD, show increased expression of zDHHC enzymes and elevated levels of S-palmitoylation of proteins regulating synaptic plasticity and $A\beta$ metabolism at an early phase of disease. We also documented the beneficial effects of the palmitoylation inhibitor 2-bromopalmitate (2-BP) on synaptic plasticity and cognitive deficits, $A\beta$ deposition, and lifespan in both male and female 3 \times Tg-AD mice. Moreover, hippocampal shRNA-mediated downregulation of zDHHC7 counteracted $A\beta$ deposition and the onset

Significance

S-palmitoylation is a protein post-translational modification regulating protein localization and catalyzed by zinc finger DHHC domain containing (zDHHC) S-acyltransferases. Aberrant protein S-palmitoylation has been reported to play a pivotal role in the brain insulin resistance (BIR)-dependent cognitive decline. The molecular crosstalk between alteration of insulin signaling and neurodegeneration has been extensively investigated, so that Alzheimer's disease (AD) has also been named type III diabetes. Here, we show that BIR epigenetically causes zDHHC7 overexpression and induces aberrant S-palmitoylation of proteins regulating synaptic function and amyloid- β metabolism. Moreover, we identified age-dependent changes of zDHHC expression in both wild-type and AD mice. Interestingly, both pharmacological and genetic inhibition of protein S-palmitoylation counteract the onset and progression of AD-related phenotype.

Author contributions: S.F. designed research; F.N., M.S., M.R., W.G., I.N.S., and G.A. performed research; F.N., D.P., and S.F. analyzed data; and S.F. and C.G. wrote the paper.

The authors declare no competing interest.

This article is a PNAS Direct Submission.

Copyright © 2024 the Author(s). Published by PNAS. This open access article is distributed under [Creative Commons Attribution-NonCommercial-NoDerivatives License 4.0 \(CC BY-NC-ND\)](https://creativecommons.org/licenses/by-nc-nd/4.0/).

¹F.N. and M.S. contributed equally to this work.

²To whom correspondence may be addressed. Email: salvatore.fusco@unicatt.it.

This article contains supporting information online at <https://www.pnas.org/lookup/suppl/doi:10.1073/pnas.2402604121/-/DCSupplemental>.

Published November 26, 2024.

of cognitive impairment in the same experimental model. Finally, enhanced expression of zDHHC7 and elevated S-palmitoylation levels of SNAP25 and BACE1 were found in the post-mortem hippocampi of AD patients. Our findings reveal a critical role of aberrant protein S-palmitoylation in the onset and progression of AD and provide evidence for developing therapeutic approaches targeting zDHHC enzymes.

Materials and Methods

Ethics Approval. The animal study protocol was approved by the Ethics Committee of Università Cattolica del Sacro Cuore (authorization no. 577/2019-PR of 29 July 2019) and was fully compliant with Italian (Ministry of Health guidelines, Legislative Decree No. 116/1992) and European Union (Directive 2010/63/EU for animal experiments) legislations on animal research.

Animals. Male and female wild type (WT) (B6129SF2/J) and 3×Tg-AD mice (3 mo old), derived from the Animal Facility of Catholic University. For in vivo experiments, mice were either intranasally injected with: i) saline solution (vehicle) and ii) 2-BP starting from 3 mo of age until 6, 9, 12 mo of age or until natural death and were weighed weekly.

Human Samples. Human post-mortem hippocampal tissues were obtained from pathologist confirmed AD cases and noncognitively impaired controls (n = 9 per each group). These samples were selected to ensure that groups were sex and age matched. Tissues were obtained by the application from the South West Dementia Brain Bank (University of Bristol, Bristol, UK) and Medical Research Council (MRC) London Brain Bank for Neurodegenerative disease (King's College London, London, UK). Data about human patients [i.e., age, post-mortem delay, Braak stage, and Mini Mental State Examination (MMSE) values] are reported in *SI Appendix, Table S1*.

Western Blotting and Silver Staining Assay. Hippocampal murine and human tissues were lysed in ice-cold lysis buffer (NaCl 150 mM, Tris-HCl 50 mM pH 8, and ethylenediaminetetraacetic acid (EDTA) 2 mM) containing 1% Triton X-100, 0.1% SDS, 1× protease inhibitor cocktail (Sigma-Aldrich), 1 mM sodium orthovanadate (Sigma-Aldrich), and 1 mM sodium fluoride (Sigma-Aldrich). Equal amounts of protein were diluted in Laemmli buffer, boiled, and resolved by sodium dodecyl-sulfate polyacrylamide gel electrophoresis (SDS-PAGE) as previously described (12). Primary antibodies (available in *SI Appendix, Table S2*) were diluted 1:1,000, incubated overnight, and revealed with horseradish peroxidase-conjugated secondary antibodies (Cell Signaling Technology Inc., Danvers, MA). Protein expression was evaluated and documented by UVitec Cambridge Alliance. Images shown were cropped for presentation with no manipulations. Silver staining assay was performed on polyacrylamide gels after SDS-PAGE following manufacturer's instructions (ProteoSilver Plus Silver Stain Kit, Sigma-Aldrich).

Acyl-Biotin Exchange Assay. Acyl-biotin exchange assay (ABE) assay was performed as previously described (4). Tissues were lysed in a buffer containing 150 mM NaCl, 50 mM Tris, 5 mM EDTA, pH 7.4, 0.2% SDS, and 1.7% Triton X-100, with 1× protease inhibitor cocktail (Sigma-Aldrich) and 10 mM NEM. After three chloroform-methanol precipitations, pellets were resuspended in a buffer containing 4% SDS, 0.7 M hydroxylamine (HAM) and incubated for 1 h at room temperature. After a chloroform-methanol precipitation, the pellets were resuspended in a buffer containing EZ-Link (N-[6-(biotinamido)hexyl]-3'-(2'-pyridyl)dithio)propionamide) (HPDP-biotin) and incubated for 1 h at room temperature. Unreacted HPDP-biotin was removed by chloroform-methanol precipitation and pellets were resuspended in lysis buffer. Samples were diluted to 0.1% SDS and biotinylated proteins were affinity-purified using streptavidin-agarose beads. Beta-mercaptoethanol (1%) was used to cleave HPDP-biotin and release biotinylated proteins from the beads. Proteins were then denatured in sample buffer and analyzed using SDS-PAGE. Palmitoylated fraction of the proteins has been calculated by densitometric analysis of the ratio palm-protein X/total protein X/total housekeeping protein (i.e., HAM⁺ protein X/protein X in the input/housekeeping protein in the input). Only for data shown in Figs. 1C and 6B and *SI Appendix, Fig. S4A*, the total amount of palmitoylated proteins (whose expression was significantly changed in hippocampi) has been calculated by densitometric analysis of the ratio palm-protein X/total housekeeping protein (i.e. HAM⁺ protein X/housekeeping protein in the input). A list of antibodies is available in *SI Appendix, Table S2*.

Real-Time PCR. Quantitative real-time PCR (qRT-PCR) amplifications were performed using Power SYBR[®] Master Mix on AB7500 instrument (Life Technologies) according to the manufacturer's instructions. The threshold values determined by the software were used to calculate transcript expression levels employing the cycle-at-threshold (Ct) method. The data are expressed as fold changes (compared to control) for each amplicon, using the 2^{-ΔΔCt} approach. The primer list is shown in *SI Appendix, Table S3*.

Chromatin Immunoprecipitation (ChIP). ChIP assays were performed as previously described (13). Tissues were resuspended in 200 μL lysis buffer containing 1% SDS, 50 mM Tris-HCl pH 8.0, and 10 mM EDTA and sonicated on ice with six 10-s pulses with a 20-s interpulse interval. About 2 μg of specific antibody or control IgG were added overnight at 4 °C. Chromatin fragments were extracted with a PCR DNA fragments purification kit (Geneaid). Primers used for zDHHC7 promoter analysis are shown in *SI Appendix, Table S4*.

Behavioral Experiments. All behavioral tests were performed as previously described (14). Recognition memory was assessed by novel object recognition (NOR) test. Short term spatial memory was investigated by Object Place Recognition (OPR) test. To identify the presence of a cognitive deficit in the NOR and OPR tests the procedures reported in Akkerman et al., were followed (15). In both tests, a population showing a 50% preference index during the test phase suggests no preference for any of the objects, thereby indicating no memory. Therefore, to analyze which condition was able to remember the previously encountered object or previously observed location, each group was confronted with a, by definition, nondiscriminating group, characterized by a mean P.I. of 50% and an 8% SD. Such group was derived from the training phase of the NOR test and selected for being the group with the highest SD. Each experimental group was then confronted with the nondiscriminating group using Welch's *t* test.

Statistical Analysis. Sample sizes were chosen with adequate power (0.8) according to results of prior pilot datasets or studies, including our own, that used similar methods or paradigms. Sample estimation and statistical analysis were performed using SigmaPlot 12 software. The statistical tests employed in the experiments (i.e., Student's *t* test, one-way ANOVA, two-way ANOVA, Pearson correlation coefficient) and eventual post hoc multiple analyses are stated in the corresponding figure legends. Kaplan-Meier curves were analyzed by log rank test. All statistical tests were two-tailed and the level of significance was set at 0.05. Results are shown as mean ± SEM.

Results

3×Tg-AD Hippocampi Show Higher Levels of Protein S-Palmitoylation. Molecular mechanisms underlying the development and progression of neurodegeneration in AD remain poorly understood (16). Protein dyshomeostasis has been recognized to play a key role in neurodegenerative disorders (17). Recently, S-palmitoylation of proteins involved in Aβ pathway, such as APP and BACE1, has been reported to enhance the generation of synaptotoxic Aβ oligomers (18, 19). To investigate the role of aberrant protein S-palmitoylation in AD, we started analyzing the whole pattern of S-palmitoylation in hippocampi of an AD experimental model at an early stage of disease. The ABE assay revealed enhanced levels of total protein S-palmitoylation in the hippocampus of both male and female 6-mo-old 3×Tg-AD mice compared to controls (+138.3%, $P = 3.39 \times 10^{-6}$; Fig. 1A).

We also evaluated the S-palmitoylation levels of a large number of proteins involved in synaptic plasticity and amyloidogenic pathway regulation. Accordingly, we found an increase of palmitoylated fraction of numerous synaptic proteins in 3×Tg-AD hippocampi compared to WT tissues (GABAγ2a receptor: +61.2%, $P = 7.62 \times 10^{-6}$; NSF: +76.5%, $P = 4.59 \times 10^{-6}$; BACE1: +111.1%, $P = 4.12 \times 10^{-4}$; CAMKIIα: +141.9%, $P = 3.16 \times 10^{-4}$; PICK1: 131.7%, $P = 3.78 \times 10^{-4}$; GRIK2: +38.2%, $P = 0.043$; GRIN2B: +209.5%, $P = 3.28 \times 10^{-8}$; SNAP25: +54.3%, 0.0081; Fig. 1B). Conversely, the S-palmitoylation levels of RAC1, PSD95, and SEPT8 were not significantly changed in 3×Tg-AD hippocampi

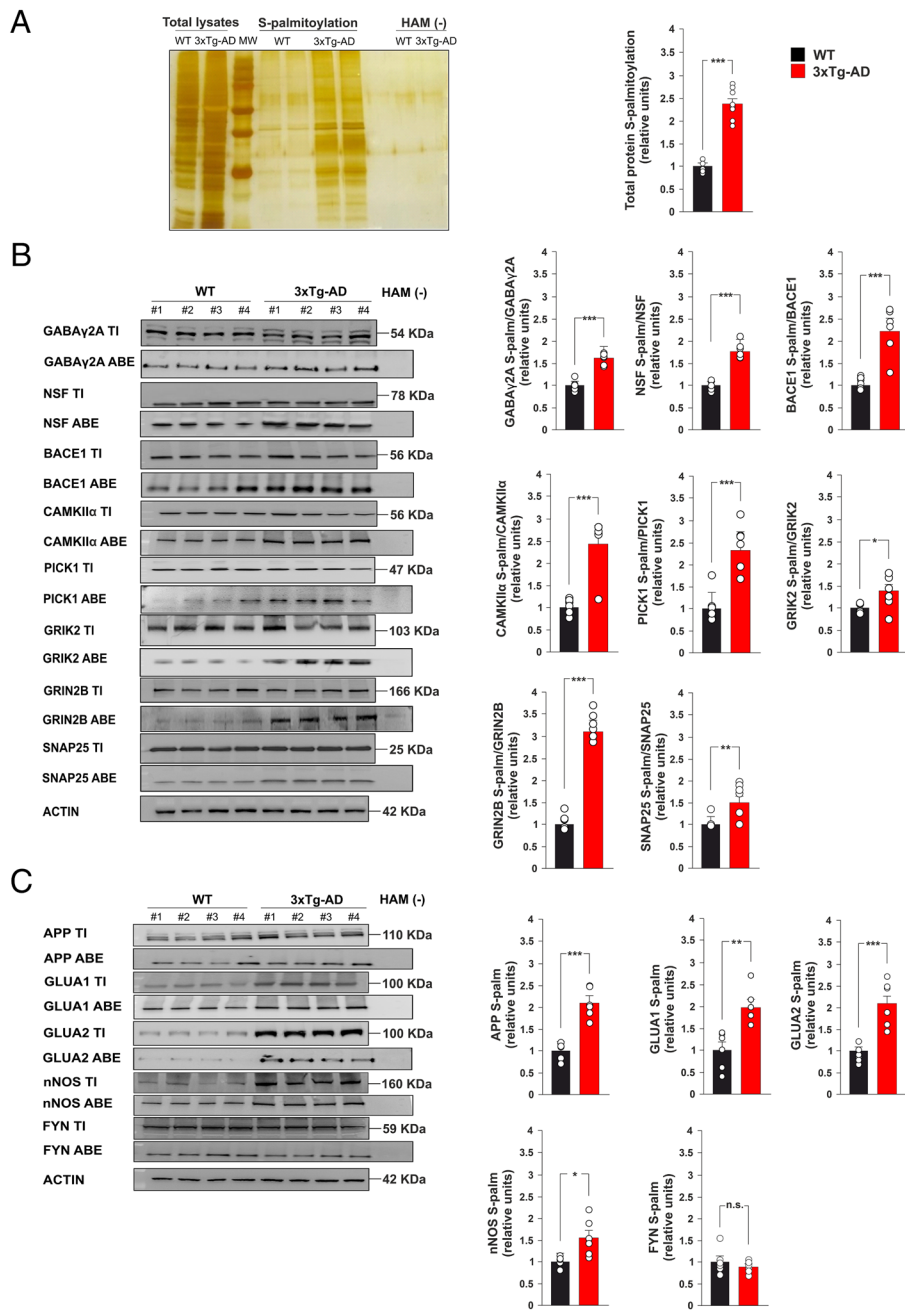


Fig. 1. Hippocampus of 3xTg-AD mice shows elevated levels of protein S-palmitoylation. (A) Silver staining assay and bar graph showing total protein S-palmitoylation in the hippocampus of WT and 3xTg-AD mice ($n = 8$ mice per group composed by males and females, statistics by unpaired Student's t test). (B) Immunoblots and bar graphs showing increase of S-palmitoylated fraction of GABA γ 2A, NSF, BACE1, CaMKII α , PICK1, GRIK2, GRIN2B, and SNAP25 ($n = 6$ mice per group composed by males and females, statistics by unpaired Student's t test). Palmitoylated fraction of the proteins has been calculated by the ratio palm-protein X/total protein X (i.e., HAM⁺ protein X/protein X in the input). (C) Immunoblots and bar graphs showing elevated levels of both palmitoylated and total APP, GluA1, GluA2, and nNOS ($n = 6$ mice per group composed by males and females, statistics by unpaired Student's t test). Palmitoylated protein levels have been calculated by the ratio palm-protein X/total housekeeping protein (i.e., HAM⁺ protein X/housekeeping protein in the input). Protein S-palmitoylation has been examined using the ABE assay (see *Acyl-Biotin Exchange Assay* section in *Methods*). Immunoblots show palmitoylated (acyl-biotin exchanged and affinity purified by streptavidin) proteins and total proteins (Total Input, TI). Samples without HAM (NH_2OH) are negative controls (-). Data are expressed as mean \pm SEM. * $P < 0.05$; ** $P < 0.01$; *** $P < 0.001$; n.s. not significant.

(SI Appendix, Fig. S1A). Moreover, APP, GluA1, GluA2, and nNOS showed elevated levels of S-palmitoylated isoform of protein together with enhanced protein expression (APP: +107.9%, $P = 5.26 \times 10^{-5}$; GluA1: +98.2%, $P = 0.0019$; GluA2: +131.1, $P = 0.0004$; nNOS: +55.3%, $P = 0.012$; Fig. 1C), whereas no significant changes were observed for Fyn. Taken together, these results suggested a potential role of aberrant protein S-palmitoylation in the development of AD phenotype.

2-BP Counteracts AD-Related Synaptic Plasticity and Cognitive Deficits. We previously demonstrated the ability of the palmitoylation inhibitor 2-BP to counteract the hyperpalmitoylation-related synaptic plasticity and memory deficits in an experimental model of cognitive decline (4). To corroborate the critical role of aberrant protein S-palmitoylation in AD and evaluate the therapeutic efficacy of 2-BP on AD-related cognitive impairment, we carried out a pharmacological study on a large cohort of both male and female 3xTg-AD mice. We intranasally treated the 3xTg-AD animals with

vehicle (veh) or 2-BP, starting from 3 to 4 mo of age (when the AD phenotype is not manifested yet), and evaluated the cognitive function at 6 mo of age, when the memory deficits begin in 3xTg-AD mice, and again at 9 and 12 mo, when memory impairment is progressively more evident in both sex of our experimental model (Fig. 2A).

Administration of 2-BP counteracted the onset and progression of memory deficits in both males and females evaluated by NOR and OPR tasks. In particular, 3xTg-AD male mice showed normal recognition memory at 6 mo and a significant impairment of discrimination index in both NOR and OPR tasks at 9 and 12 mo, whereas 2-BP-treated 3xTg-AD animals still maintained a discrimination capacity in both tasks at each stage (NOR preference index: 60.1% with $P = 0.0092$ for 3xTg-AD_{veh} and 71.8% with $P = 1.77 \times 10^{-5}$ for 3xTg-AD_{2BP} at 6 mo, 53.5% with $P = 0.3111$ for 3xTg-AD_{veh} and 63.3% with $P = 7.6 \times 10^{-4}$ for 3xTg-AD_{2BP} at 9 mo, 52% with $P = 0.5603$ for 3xTg-AD_{veh} and 63.2% with $P = 7.3 \times 10^{-4}$ for 3xTg-AD_{2BP} at 12 mo; OPR

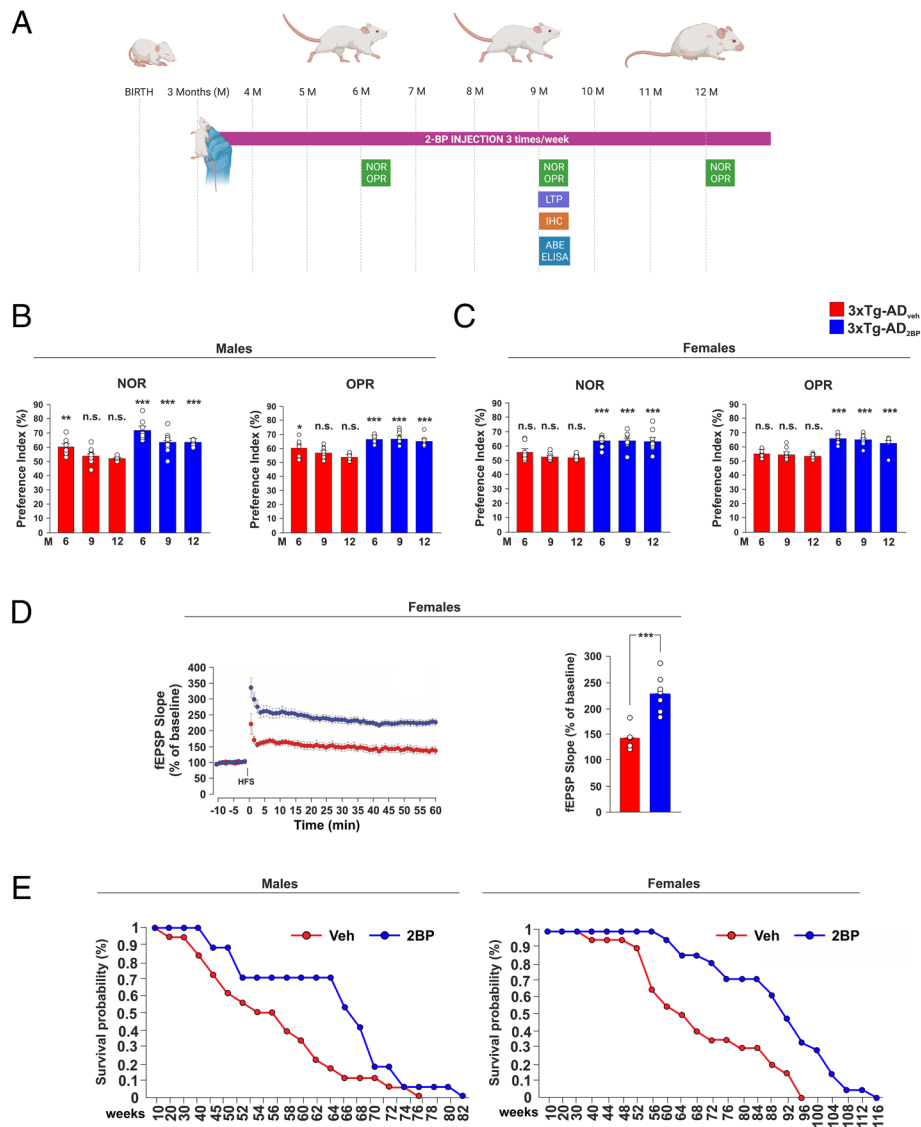


Fig. 2. Intranasal administration of 2-BP relieves AD phenotype in 3xTg-AD mice. (A) Timeline of experimental design (pharmacological treatment, molecular, electrophysiological, and behavioral analyses). Preference index of (B) male and (C) female 3xTg-AD mice intranasally treated with either saline (veh) or 2-BP for 3, 6, or 9 mo in both NOR and OPR tests ($n = 8$ to 12 males and 8 to 10 females per group; statistics by Welch's t test). (D) Time course (Left) and bar graph (Right) showing slope of LTP at CA3-CA1 synapses in hippocampal slices obtained from vehicle- and 2-BP-treated female 3xTg-AD mice (3xTg-AD_{veh} and 3xTg-AD_{2BP}, respectively). Results are expressed as percentages of baseline ($n = 12$ slices from $n = 5$ mice for 3xTg-AD_{veh} and $n = 13$ slices from $n = 7$ mice for 3xTg-AD_{2BP}; statistics by unpaired student's t test). (E) Kaplan-Meier survival curve comparing survival probability of vehicle (veh)- and 2-BP-treated male (Left) and female (Right) 3xTg-AD from 10 wk of age until death ($n = 17$ to 18 males and 20 to 21 females for each group; statistics by log rank test). Data are expressed as mean \pm SEM. ** $P < 0.01$; *** $P < 0.001$; n.s. not significant.

preference index: 60.2% with $P = 0.012$ for 3xTg-AD_{veh} and 66.7% with $P = 9 \times 10^{-5}$ for 3xTg-AD_{2BP} at 6 mo, 56.7% with $P = 0.041$ for 3xTg-AD_{veh} and 67.1% with $P = 6.4 \times 10^{-5}$ for 3xTg-AD_{2BP} at 9 mo, 53.7% with $P = 0.248$ for 3xTg-AD_{veh} and 65.1% with $P = 2.2 \times 10^{-4}$ for 3xTg-AD_{2BP} at 12 mo; Fig. 2B). 2-BP slowed down the onset and progression of cognitive deficits also in 3xTg-AD female mice, which showed altered performance in both recognition and spatial memory starting as early as 6 mo of age (NOR preference index: 55.7% with $P = 0.135$ for 3xTg-AD_{veh} and 63.6% with $P = 5.3 \times 10^{-4}$ for 3xTg-AD_{2BP} at 6 mo, 52.4% with $P = 0.475$ for 3xTg-AD_{veh} and 63.8% with $P = 5.4 \times 10^{-4}$ for 3xTg-AD_{2BP} at 9 mo, 52% with $P = 0.556$ for 3xTg-AD_{veh} and 63.4% with $P = 0.0018$ for 3 Tg-AD_{2BP} at 12 mo; OPR preference index: 54.9% with $P = 0.128$ for 3xTg-AD_{veh} and 65.5% with $P = 1.7 \times 10^{-4}$ for 3xTg-AD_{2BP} at 6 mo, 54.3% with $P = 0.192$ for 3xTg-AD_{veh} and 65.1% with $P = 1.8 \times 10^{-4}$ for 3xTg-AD_{2BP} at 9 mo, 53.1% with $P = 0.324$ for 3xTg-AD_{veh} and 62.3% with $P = 1.8 \times 10^{-3}$ for 3xTg-AD_{2BP} at 12 mo; Fig. 2B).

Moreover, we analyzed long-term potentiation (LTP) at CA3-CA1 synapses in hippocampal brain slices obtained 3xTg-AD female mice, who showed a more severe phenotype compared to males, at 9 mo of age when naive 3xTg-AD females showed impairment of synaptic plasticity. Accordingly, LTP was significantly higher in mice treated with 2-BP (fEPSP slope: $225.7 \pm 14.6\%$, vs. $141 \pm 11.7\%$, $P = 0.0009$; Fig. 2D). We also evaluated the effects of 2-BP intranasal administration on WT mice from both behavioral and electrophysiological point of view. Both male and female WT naive animals did not show any cognitive decline from 6 to 12 mo of age, nor memory alteration upon 2-BP treatment (for males: 65.7%, 67.1%, 65.6% for 6-, 9-, 12-mo-old WT_{veh}, respectively, and 64.4%, 66.1%, 65.9% for 6-, 9-, 12-mo-old WT_{2BP}, respectively, as NOR preference index, $P < 0.001$ in all experimental conditions; 66.6%, 66.1%, 65.6% for 6-, 9-, 12-mo-old WT_{veh}, respectively, and 66.1%, 67.4%, 66.1% for 6-, 9-, 12-mo-old WT_{2BP}, respectively, as OPR preference index, $P < 0.001$ in all experimental conditions; for females: 65.7%, 66.3%, 64.9% for

6-, 9-, 12-mo-old WT_{veh}, respectively, and 65.3%, 66.3%, 66.1% for 6-, 9-, 12-mo-old WT_{2BP}, respectively, as NOR preference index, $P < 0.001$ in all experimental conditions; 66.3%, 66.9%, 64.7% for 6-, 9-, 12-mo-old WT_{veh}, respectively, and 66.8%, 65.3%, 64.6% for 6-, 9-, 12-mo-old WT_{2BP}, respectively, as OPR preference index, $P < 0.001$ in all experimental conditions; *SI Appendix, Fig. S2A*). Accordingly, we did not detect any significant change of LTP amplitude or slope at CA3-CA1 hippocampal synapses of 9-mo-old female WT mice upon chronic 2-BP administration (fEPSP slope: $181.5 \pm 10.7\%$, vs. $174.6 \pm 8.6\%$, $P = 0.326$; *SI Appendix, Fig. S2B*). To more extensively investigate the effect of 2-BP on 3×Tg-AD mice, we also evaluated both weight and food intake of animals, but no significant changes were observed upon the S-palmitoylation inhibitor administration (*SI Appendix, Fig. S2C*). It has been reported that 3×Tg-AD mice exhibited elevated levels of anxiety in the progression of disease (20, 21). Therefore, we also analyzed the effects of 2-BP on anxiety-related behaviors. Upon 2-BP treatment, 3×Tg-AD mice did not show any significant change of behavioral performance in EPM, DLB, and OF tests at 9 and 12 mo of age with respect to age-matched AD mice treated with vehicle (for DLB test: in 9-mo-old male mice $F_{2,96} = 83.18$, dark vs. light box in 3×Tg-AD_{veh} $P = 3.19 \times 10^{-10}$, dark vs. light box in 3×Tg-AD_{2BP} $P = 7.65 \times 10^{-11}$; in 12-mo-old mice $F_{2,96} = 110.2$, dark vs. light box in 3×Tg-AD_{veh} $P = 2.9 \times 10^{-10}$, dark vs. light box in 3×Tg-AD_{2BP} $P = 3.51 \times 10^{-13}$; in 9-mo-old female mice $F_{2,96} = 121.38$, dark vs. light box in 3×Tg-AD_{veh} $P = 2.67 \times 10^{-13}$, dark vs. light box in 3×Tg-AD_{2BP} $P = 5.16 \times 10^{-11}$; in 12-mo-old female mice $F_{2,96} = 238.17$, dark vs. light box in 3×Tg-AD_{veh} $P = 8.13 \times 10^{-14}$, dark vs. light box in 3×Tg-AD_{2BP} $P = 4.36 \times 10^{-15}$; *SI Appendix, Fig. S2 D–F*). Considering the long-term beneficial effects of 2-BP on cognitive functions, we evaluated the impact of the palmitoylation inhibitor on the survival of large cohorts of 3×Tg-AD mice. It has been reported that both male and female 3×Tg-AD mice showed a shorter lifespan compared to WT mice (22). Of note, 2-BP extended life expectancy in both male and female 3×Tg-AD mice ($P = 0.011$ for males, $P = 0.007$ for females; Fig. 2E). Collectively, our data demonstrated that intranasal administration of 2-BP counteracted the onset and progression of AD-related synaptic and memory deficits and increased the lifespan in 3×Tg-AD mice.

2-BP Reduces the Aβ 1 to 42 Levels in the Hippocampus of 3×Tg-AD Mice. To better understand the molecular changes underlying the beneficial effects of 2-BP on AD phenotype, we first analyzed the pattern of protein S-palmitoylation in the hippocampus of 3×Tg-AD mice upon 2-BP treatment (hereinafter named 3×Tg-AD_{2BP} mice). 2-BP reduced the levels of total protein S-palmitoylation in the hippocampus after 6 mo of treatment without completely reverting them to levels detected in the hippocampus of WT mice (-50.6% , $P = 7.4 \times 10^{-5}$; Fig. 3A).

Because 3×Tg-AD model progressively develop Aβ and tau pathology (23), we investigated the effect of 2-BP intranasal administration on these AD molecular hallmarks. The pharmacological treatment reduced Aβ deposition in the hippocampus compared to controls. Enzyme-linked immunosorbent assay (ELISA) showed low Aβ 1 to 42 levels in both male and female 9-mo-old mice (males: 158.7 ± 5 pg/mL vs. 208.2 ± 6.2 pg/mL, $P = 1.1 \times 10^{-4}$; females: $2,915.9 \pm 293.7$ pg/mL vs. $4,599.3 \pm 487.6$ pg/mL, $P = 0.0088$; Fig. 3B). Accordingly, both immunofluorescence and western blotting experiments detected lower levels of Aβ isoforms in the hippocampal tissues of 3×Tg-AD_{2BP} mice (IHC: -34.6% , $P = 2.4 \times 10^{-5}$; WB: -73% $P = 5.6 \times 10^{-5}$; Fig. 3 C and D). Conversely, no significant changes of tau phosphorylation were detected in the same brain tissues (Fig. 3E). To investigate the effect of 2-BP administration on Aβ

deposition in other brain regions, we first evaluated the expression of hAPP transgene in 3×Tg-AD brain. We detected higher expression of hAPP in both amygdala and parahippocampal cortex as well as the hippocampus (*SI Appendix, Fig. S3A*). Immunofluorescence analysis showed no significant difference of Aβ immunoreactivity in the amygdala of 3×Tg-AD_{2BP} mice, whereas lower levels of Aβ were detected in the parahippocampal cortex of the same mice compared to untreated animals (*SI Appendix, Fig. S3B*). Moreover, western blotting analysis confirmed lower expression of Aβ in the parahippocampal cortex of 3×Tg-AD_{2BP} mice (*SI Appendix, Fig. S3C*). Taken together, our data confirmed that 2-BP reduced protein S-palmitoylation levels in the hippocampus and Aβ deposition in both hippocampus and parahippocampal cortex of 3×Tg-AD mice.

Hippocampal zDHHC7 Silencing Prevents the Onset of Cognitive Impairment in 3×Tg-AD Mice. To gain insight into the molecular mechanisms underlying the crosstalk between S-palmitoylation and neurodegeneration, we analyzed the expression of a group of zDHHCs regulating synaptic plasticity or targeting enzymes involved in Aβ metabolism in the hippocampus of WT and 3×Tg-AD mice at different stages (7–10, 24–26). mRNA analysis revealed higher levels of several zDHHC enzymes in the hippocampus of 3×Tg-AD mice compared to WT animals ($F_{3,28} = 67.48$ for zDHHC5: $+70\%$ at 3 mo, $P = 0.015$; $F_{3,28} = 146.1$ for zDHHC7: $+250\%$ at 3 mo, $P = 8.62 \times 10^{-5}$, $+841.2\%$ at 9 mo, $P = 2.66 \times 10^{-5}$; $F_{3,28} = 13.98$ for zDHHC13: $+113\%$ at 3 mo, $P = 0.0024$, $+60.7\%$ at 9 mo, $P = 0.0045$; $F_{3,28} = 6.00$ for zDHHC20: $+61\%$ at 3 mo, $P = 0.0056$, $+35.2\%$ at 9 mo, $P = 0.038$; $F_{3,28} = 84.37$ for zDHHC21: $+260\%$ at 3 mo, $P = 3.73 \times 10^{-6}$, $+436.6\%$ at 9 mo, $P = 2.92 \times 10^{-5}$; Fig. 4A). We also analyzed the changes of zDHHC enzymes at protein levels and we found higher expression of both zDHHC7 and zDHHC21 in the hippocampi of 3×Tg-AD mice compared to WT at 3 mo of age when the AD phenotype is not yet manifest (zDHHC7: $+89.9\%$, $P = 0.017$; zDHHC21: $+113.8\%$, $P = 0.0005$; Fig. 4B). Autopalmitoylation can occur for some zDHHC enzymes and the S-palmitoylation modification has been reported to activate zDHHC7. So, we investigated the S-palmitoylation of both zDHHC7 and zDHHC21 in the hippocampus of 3×Tg-AD mice and we found an increase of zDHHC7 S-palmitoylation levels compared to WT ($+102.6\%$, $P = 0.00126$; *SI Appendix, Fig. S4A*), whereas no palmitoylation signal was detectable for zDHHC21. In addition, we evaluated the expression of both S-acyltransferases in the parahippocampal cortex of both 3-mo-old 3×Tg-AD and WT mice but we did not detect any significant change (*SI Appendix, Fig. S4B*). Moreover, we investigated whether 2-BP treatment affected the expression of both zDHHC7 and zDHHC21 in the hippocampus of 3×Tg-AD mice after 6 mo of administration. Western blotting analysis did not show any significant change of S-acyltransferase expression upon 2-BP treatment (*SI Appendix, Fig. S4C*).

Thus, we downregulated the expression of either zDHHC7 or zDHHC21 in the hippocampus of 3×Tg-AD mice to evaluate the role of palmitoyl transferase enzymes in the onset of cognitive deficits. Four-month-old 3×Tg-AD female mice were stereotaxically injected with lentiviral particles harboring short hairpin RNA sequences against zDHHCs (hereinafter defined LV-sh zDHHC7 and LV-sh zDHHC21 mice) and were evaluated by both NOR and OPR tests at 6 mo of age. LV-sh zDHHC7 mice showed higher cognitive performance in both behavioral tasks compared to animals injected with lentiviral vector expressing scrambled shRNA (NOR preference index: 66.9% and $P = 6.07 \times 10^{-5}$ for LV-sh zDHHC7 mice, 53.6% and $P = 0.658$ for LV-sh scrambled mice; OPR preference index: 62.8% and $P = 0.012$ for LV-sh zDHHC7 mice, 52.4% and $P = 0.681$ for LV-sh scrambled mice; Fig. 4C). Conversely,

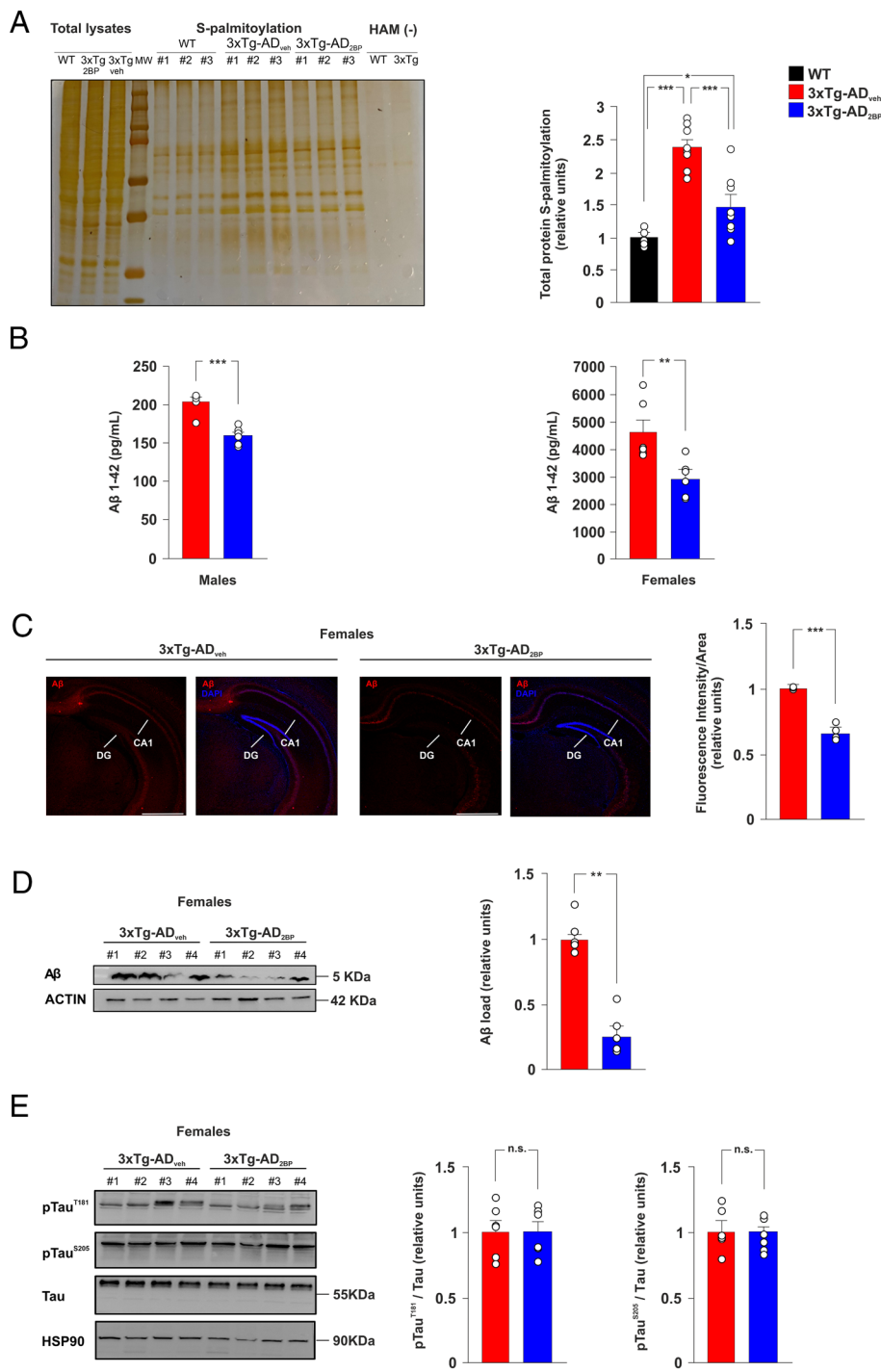


Fig. 3. 2-BP reduces protein S-palmitoylation and A β levels in 3xTg-AD hippocampi. (A) Silver staining assay and bar graph showing total protein S-palmitoylation in the hippocampus of WT, 3xTg-AD_{veh} and 3xTg-AD_{2BP} mice (n = 8 mice per group composed by males and females, statistics by unpaired Student's *t* test). (B) A β 1 to 42 peptide levels (pg of A β per mg of total proteins) in the hippocampus of male (Left) and female (Right) 3xTg-AD_{veh} and 3xTg-AD_{2BP} mice. ELISA was performed in triplicate (n = 6 mice; statistics by unpaired Student's *t* test). (C) Immunostaining (Left) and bar graph (Right) showing A β load in the hippocampus of female 3xTg-AD_{veh} and 3xTg-AD_{2BP} animals (n = 6 mice, five slices have been analyzed for each animal; statistics by unpaired Student's *t* test; (Scale bar: 250 μ m.) Immunoblots (Left) and bar graphs (Right) showing (D) A β load and (E) tau phosphorylation levels in the hippocampus of female 3xTg-AD_{veh} and 3xTg-AD_{2BP} mice (n = 6 mice; statistics by unpaired Student's *t* test). Data are expressed as mean \pm SEM. ***P* < 0.01; ****P* < 0.001; n.s. not significant.

zDHHHC21 silencing in 3xTg-AD mice as well as zDHHHC7 silencing in WT mice did not show any significant change in terms of cognitive performance compared to controls (Fig. 4C and *SI Appendix*, Fig. S4G). Immunofluorescence and western blotting experiments confirmed the expression of gene reporter enclosed in lentiviral vectors in CA1 region and the specificity of shRNAs against zDHHHCs (*SI Appendix*, Fig. S4 D–F). Moreover, western blotting analysis revealed reduced expression of both zDHHHC7 and zDHHHC21 in the hippocampi of silenced mice (–47.4% and *P* = 0.0038 for zDHHHC7, –64.4% and *P* = 3.4×10^{-6} for zDHHHC21; Fig. 4D). We also investigated the S-palmitoylation levels of zDHHHC7 targets in the hippocampus of LV-sh zDHHHC7 3xTg-AD mice and found hypopalmitoylation of BACE1, SNAP25, nNOS, and γ 2 subunit of GABA_A receptor (–67% and *P* = 9.6×10^{-4} for

BACE1, –55% and *P* = 0.041 for SNAP25; –75% and *P* = 0.0019 for nNOS; –35% and *P* = 0.0068 for GABA_A γ 2; Fig. 4E), whereas no change was detected in zDHHHC7-silenced hippocampi of WT mice (*SI Appendix*, Fig. S4G). Finally, A β 1 to 42 levels were reduced in the hippocampus of LV-sh zDHHHC7 3xTg-AD mice ($1,514.1 \pm 98.1$ pg/mL vs. $2,869.9 \pm 208.9$ pg/mL, *P* = 7.5×10^{-5} ; Fig. 4F). Collectively, these findings revealed a key role of zDHHHC7 in the development of both A β deposition and cognitive impairment in 3xTg-AD mice.

Expression of zDHHHC7 Is Epigenetically Upregulated in 3xTg-AD Hippocampi. To date, understanding of the mechanisms underlying regulation of zDHHHC expression is still limited. We previously demonstrated that alteration of brain insulin

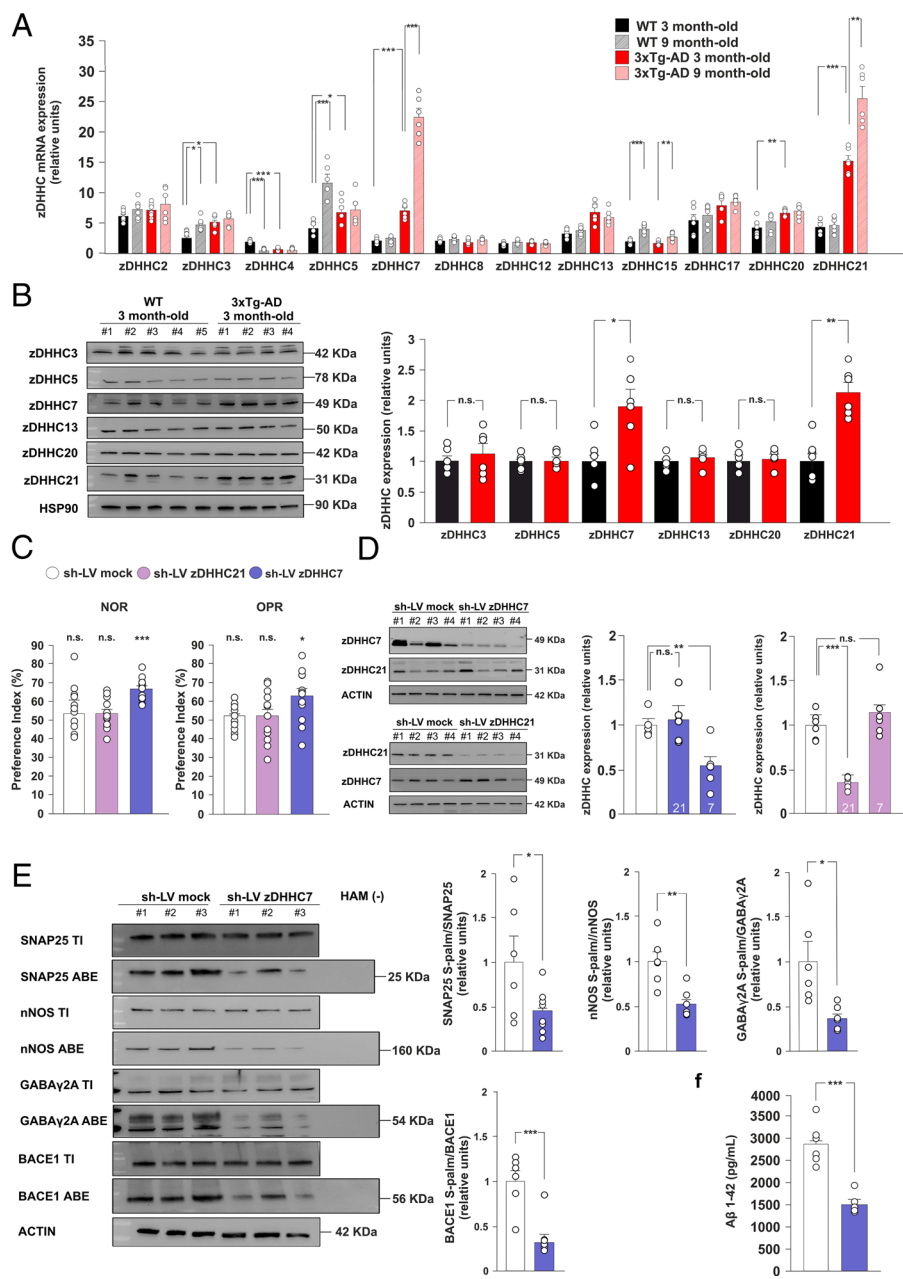


Fig. 4. zDHHHC7 silencing counteracts A β deposition and the onset of cognitive deficits in 3 \times Tg-AD mice. (A) mRNA expression of different zDHHHC enzymes (2–5, 7, 8, 12, 13, 15, 17, 20, 21) in both WT and 3 \times Tg-AD mice at 3 and 9 mo of ages ($n = 6$ mice for each group composed by males and females; statistics by two-way ANOVA and Bonferroni post hoc). (B) Immunoblot (Left) and bar graph (Right) showing protein expression of zDHHHCs 3, 7, and 21 in WT vs. 3 \times Tg-AD young mice ($n = 6$ mice for each group composed by males and females; statistics by unpaired Student's t test). (C) Preference index in NOR (Left) and OPR (Right) tests of 3 \times Tg-AD mice stereotactically injected with lentiviral particles encoding a shRNA targeting zDHHHC7 (LV-sh zDHHHC7), zDHHHC21 (LV-sh zDHHHC21), or control lentiviral particles (LV-sh scrambled, mock) ($n = 10$ to 13 female mice per group; statistics by Welch's t test). (D) Immunoblots (Left) and bar graphs (Right) showing expression of zDHHHCs 7 and 21 in LV-sh zDHHHC7 and LV-sh zDHHHC21 injected mice ($n = 6$ female mice for each group; statistics by unpaired Student's t test). (E) Immunoblots and bar graphs showing S-palmitoylation of SNAP25, nNOS, GABA γ 2A, and BACE1 ($n = 6$ female mice for each group, statistics by unpaired Student's t test). (F) A β 1 to 42 levels (pg of A β per mg of total proteins) of in the hippocampus of LV-sh zDHHHC7 and mock 3 \times Tg-AD mice. ELISA was performed in triplicate ($n = 6$ female mice for each group; statistics by unpaired Student's t test). Data are expressed as mean \pm SEM. * $P < 0.05$; ** $P < 0.01$; *** $P < 0.001$; n.s. not significant.

signaling led to the epigenetic upregulation of zDHHHC3 in a mouse model of cognitive decline (4). Molecular hallmarks of BIR have been reported in AD experimental models and post-mortem brain tissues of AD patients (27, 28). To evaluate brain insulin signaling in 3 \times Tg-AD mice, we intranasally treated 3-, 6-, and 9-mo-old mice with insulin and analyzed the activation of insulin receptor downstream effectors in their hippocampi. Upon insulin administration, we observed increased phosphorylation levels of insulin receptor substrate 1 (IRS1), AKT, and GSK3 β kinases, and transcription factor FoxO1 in young 3 \times Tg-AD mice (Fig. 5A). Conversely, in the hippocampi of older 3 \times Tg-AD mice we found aberrant insulin signaling, consisting of basal hyperphosphorylation of GSK3 β , AKT, IRS1, and FoxO1 (pGSK3 β : $F_{3,28} = 6.19$ and +213.7% at 6 mo, $P = 0.0196$, $F_{3,28} = 5.91$ and +313.1% at 9 mo, $P = 0.021$; pAKT Ser473: $F_{3,28} = 6.7$ and +124.4% at 6 mo, $P = 0.0064$; pIRS1 Ser612: $F_{3,28} = 9.82$ and +112.2% at 6 mo, $P = 0.0008$, $F_{3,28} = 7.42$ and +41.9% at 9 mo, $P = 0.0307$; pFoxO1 Ser256: $F_{3,28} = 7.96$ and +96.3% at 9 mo, $P = 0.014$; Fig. 5A) and loss

of insulin-dependent phosphorylation of the same downstream effectors (Fig. 5A).

To investigate a potential FoxO1-mediated regulation of zDHHHC7 expression, we studied both the binding of FoxO1 and the epigenetic activation on the regulatory sequences of zDHHHC7 gene. Bioinformatic analysis of the mouse zDHHHC7 locus (NC_000074.7) revealed the presence of several putative FoxO responsive elements (pFRE) upstream the starting codon (pFRE1 including: -1267; pFRE2 including: -2066; pFRE3 including: -2833; Fig. 5B). CHIP from hippocampal lysates showed that FoxO1 specifically bound two of these genomic regions (pFRE2 and pFRE3), and its recruitment significantly decreased in 3 \times Tg-AD hippocampi (-79.4% on pFRE2, $P = 3.94 \times 10^{-6}$; -73.2% on pFRE3, $P = 2.92 \times 10^{-6}$; Fig. 5C). Accordingly, the transcriptional activation marker lysine 9 histone 3 acetylation was upregulated on the same regulatory sequences in AD experimental model (+181.1% on pFRE2, $P = 9.27 \times 10^{-4}$; +149.4% on pFRE3, $P = 1.43 \times 10^{-5}$; Fig. 5B). Taken together, our data indicated that aberrant expression of zDHHHC7 in the

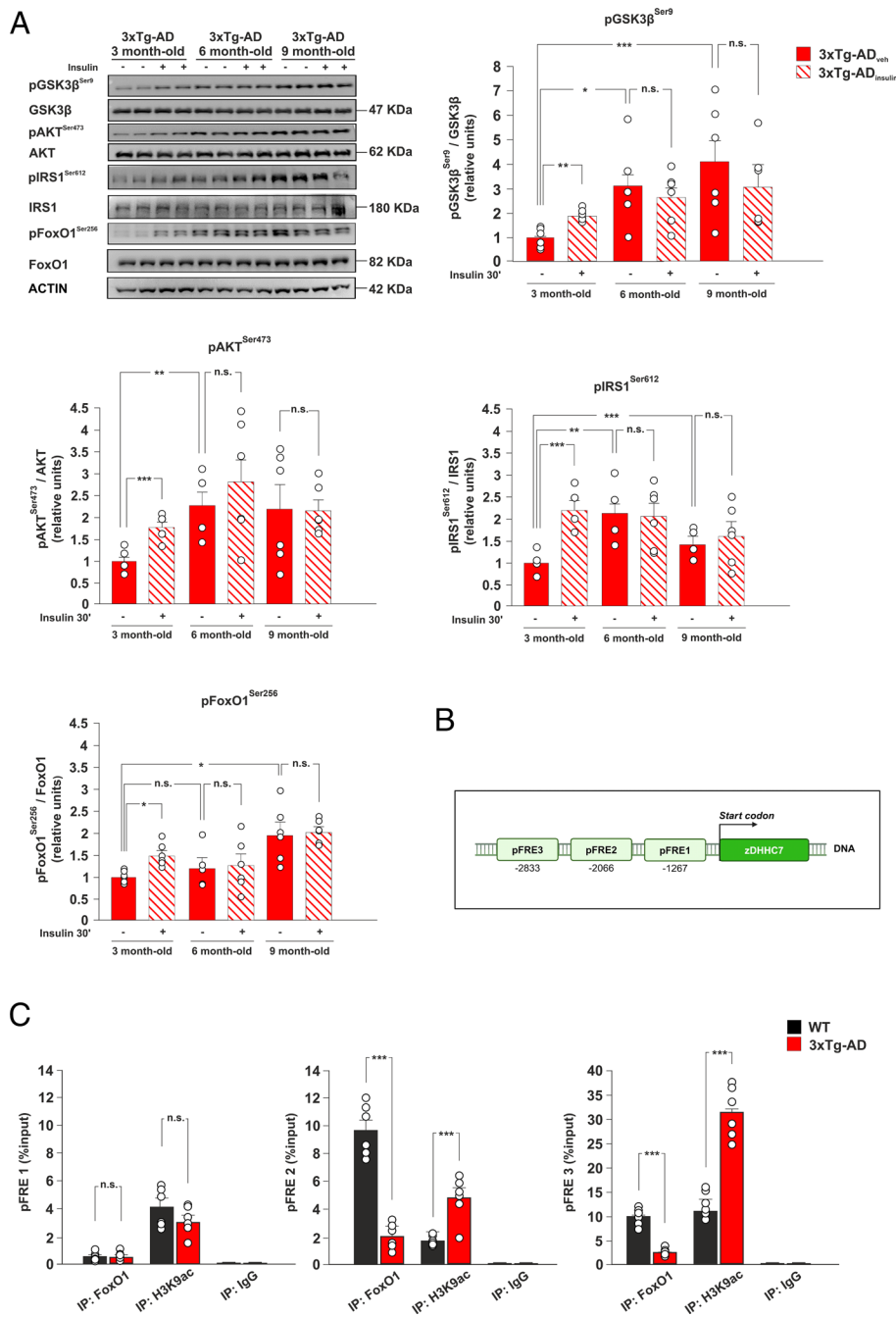


Fig. 5. FoxO1 inhibition epigenetically regulates zDHHc7 expression. (A) Immunoblots (Top) and bar graphs (Bottom) showing the responsiveness of insulin signaling pathway (GSK3βSer9, AKTSer473, IRS-1Ser612, and FoxO1 Ser256 phosphorylation) in 3-, 6-, and 9-month-old 3xTg-AD mice (n = 6 mice per group composed by males and females; statistics by unpaired Student's *t* test). (B) Scheme displaying several putative FRE elements within the mouse zDHHc7 gene. The numbers indicate the distance from the ATG starting codon. (C) ChIP assays showing the binding of FoxO1 and histone 3 lysine 9 acetylation (H3K9ac) on the regulatory sequences (FRE) of the zDHHc7 gene in the hippocampus of WT and 3xTg-AD mice at 6 mo of age. Experiments were performed in triplicate (n = 6 mice per group composed by males and females; statistics by unpaired Student's *t* test). Data are expressed as mean ± SEM. **P* < 0.05; ****P* < 0.001; n.s. not significant.

hippocampi of 3xTg-AD mice might be induced by BIR-dependent inhibition of transcription factor FoxO1 and epigenetic activation of zDHHc7 promoters.

Human AD Post-Mortem Hippocampi Show Higher Levels of ZDHHc7 Expression and BACE1 Palmitoylation. To further investigate the role of aberrant protein S-palmitoylation in AD, we analyzed zDHHc7 expression and palmitoylation levels of its molecular targets in post-mortem hippocampal tissues of AD patients. We found elevated expression of zDHHc7 protein (+127%, *P* = 0.016; Fig. 6A) together with increased levels of S-palmitoylated isoform of protein in AD hippocampi compared to nondemented (ND) patients (+48%, *P* = 0.026; Fig. 6B).

Moreover, the palmitoylated fractions of both SNAP25 and BACE1 proteins were significantly increased in the same AD brain tissues (+83% and *P* = 0.0047 for BACE1, +29% and *P* = 0.0103

for SNAP25; Fig. 6C). No significant changes were observed for APP S-palmitoylation (Fig. 6C). We also measured the Aβ 1 to 42 hippocampal load that, as expected, was significantly higher in AD hippocampi compared to controls (+1,200%, *P* = 8.1 × 10⁻⁵; Fig. 6D). Thus, we asked whether there was a statistical correlation between BACE1 S-palmitoylation and Aβ 1 to 42 levels in the hippocampus of human patients. Pearson's correlation coefficient (*r*) showed a positive and statistically significant correlation (*r* = 0.55, *P* = 0.019; Fig. 6E). More importantly, a negative and statistically significant correlation was observed comparing hippocampal BACE1 S-palmitoylation levels and MMSE scores of human patients (*r* = -0.548, *P* = 0.027; Fig. 6E and *SI Appendix, Table S1*).

In summary, our data showed an increase of both zDHHc7 expression and S-palmitoylation levels of proteins critically involved in the regulation of synaptic plasticity and Aβ metabolism in hippocampal tissues of AD patients and revealed a

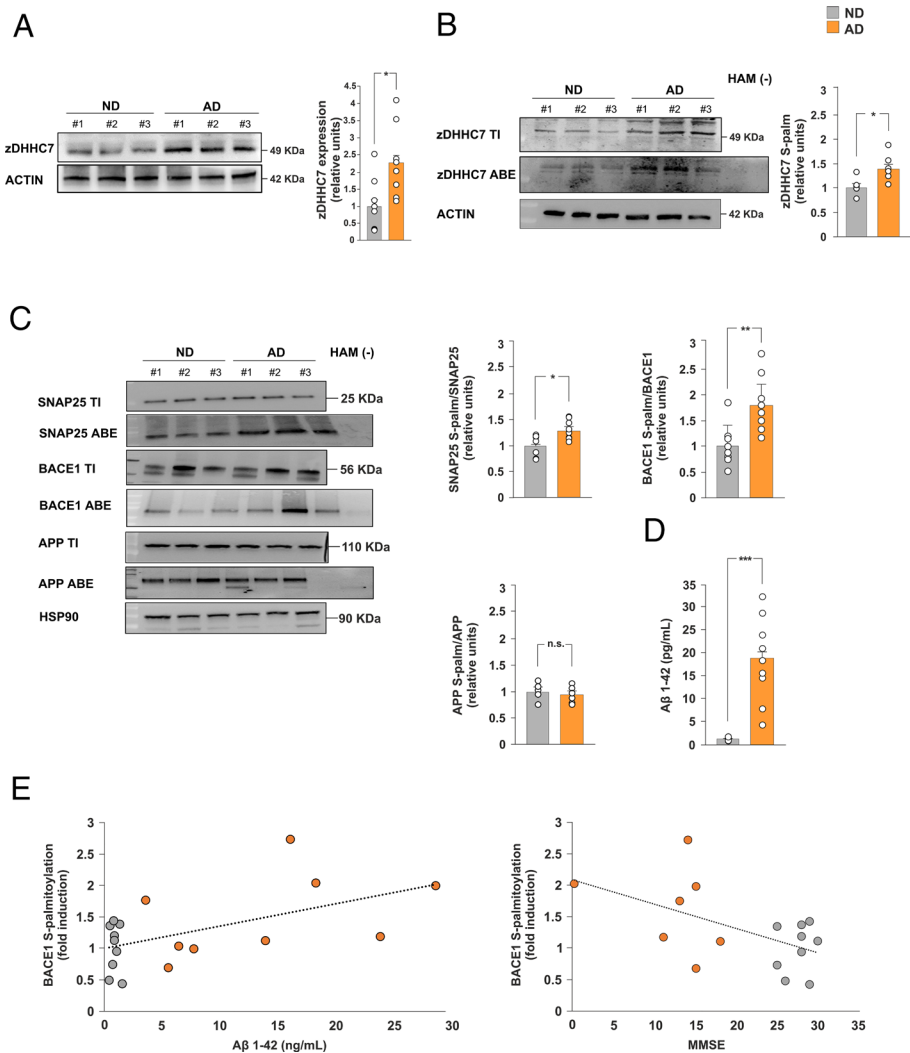


Fig. 6. Hippocampi of AD patients show increased levels of both zDHC7 expression and protein S-palmitoylation. (A) Immunoblots and bar graph showing zDHC7 expression in postmortem hippocampal tissue of ND and AD patients ($n = 9$ hippocampi; statistics by unpaired student's t test). (B) Immunoblots and bar graphs showing S-palmitoylation levels of zDHC7 in the hippocampus of ND and AD patients ($n = 9$ for each group, statistics by unpaired Student's t test). Immunoblots show palmitoylated (acyl-biotin exchanged and detected by streptavidin) proteins and total proteins (Total Input, TI). Palmitoylated protein levels have been calculated by the ratio palm-protein X/total housekeeping protein (i.e. HAM⁺ protein X/housekeeping protein in the input). (C) Immunoblots and bar graphs showing S-palmitoylation levels of BACE1, SNAP25, and APP in the hippocampus of ND and AD patients ($n = 9$ for each group, statistics by unpaired Student's t test). Immunoblots show palmitoylated (acyl-biotin exchanged and affinity purified by streptavidin) proteins and total proteins (TI). (D) A β 1 to 42 levels in the hippocampus of ND and AD patients. ELISA was performed in triplicate ($n = 9$; statistics by unpaired Student's t test). (E) Scatter plots reporting the distribution for BACE1 S-palmitoylation and A β 1 to 42 levels (on *Left*, $n = 9$ per group; statistics by Pearson correlation coefficient) or for BACE1 S-palmitoylation and MMSE values (on *Right*, $n = 9$ per group; statistics by Pearson correlation coefficient). Data are expressed as mean \pm SEM. * $P < 0.05$; ** $P < 0.01$; *** $P < 0.005$.

significant positive correlation between BACE1 S-palmitoylation and either A β deposition in human hippocampi or cognitive decline.

Discussion

AD is a pressing challenge for aging populations worldwide (29). All therapeutic attempts made so far based on current knowledge have proven scarcely effective, probably because the molecular mechanisms underlying the onset and progression of the disease still remain poorly understood (30, 31). PTMs have been clearly demonstrated to regulate synaptic function and be altered in neurological disorders (32–35). Among multiple PTMs, S-palmitoylation is fundamental in modulation of synaptic activity and its dysfunction has been reported to be associated to several neurodegenerative diseases (7, 36). We hypothesized that aberrant S-palmitoylation of proteins regulating synaptic plasticity and A β metabolism might play a critical role in the development of AD. First, we found an

increase of both total levels of protein S-palmitoylation and expression of several zDHC enzymes in the hippocampus of 3 \times Tg-AD mice at an early stage of the disease (Figs. 1A and 4B). S-palmitoylation changes of different targets may either promote or inhibit synaptic function, making it difficult to predict the effect of an increase of total protein S-palmitoylation on cognitive function of 3 \times Tg-AD mice. Indeed, higher levels of protein S-palmitoylation detected in our AD experimental model can induce conflicting effects on the localization and activity of the same target (due to the multiple cysteine residues modulated in the same protein) or by regulating in parallel inhibitory and excitatory synaptic components involved in the modulation of cognitive function. However, it has been reported that interfering with S-palmitoylation of two γ -secretase subunits, APH1 and nicastrin, reduced A β deposition in a transgenic mouse model of AD (37). Here, we investigated the effect of either pharmacological or genetic inhibition of protein S-palmitoylation on the development of synaptic and cognitive deficits. Intranasal administration of the nonspecific palmitoylation

inhibitor 2-BP, starting at 3 mo of age, delayed and relieved memory impairment in both male and female 3×Tg-AD mice (Fig. 2 *B* and *C*) and improved LTP at CA1-CA3 synapses of female animals (Fig. 2 *D* and *E*), whereas no significant effects were detected in WT mice. Moreover, 2-BP decreased both Aβ deposition and protein S-palmitoylation levels in the hippocampus of 3×Tg-AD mice (Figs. 2 *D* and *E* and 3 *A–D*). It also reduced Aβ levels in the parahippocampal cortex suggesting that beneficial effect of 2-BP against Aβ deposition is also extended to other brain regions besides the hippocampus (*SI Appendix*, Fig. S2 *B* and *C*). Certainly, 2-BP may act on numerous targets and modulate the palmitoylation of several synaptic proteins by either inhibiting zDHHC enzymes or directly competing with palmitic acid and promoting the alkylation of several palmitoylated cysteines (38). Moreover, 2-BP can inhibit both palmitoylation and depalmitoylation, along with many other cysteine modifications (38, 39). It is also worth mentioning that 2-BP impacts on other pathways including inflammation, modulation of fatty acid β-oxidation and NADPH cytochrome c reductase activity (40–42). In addition, hippocampal silencing of zDHHC7, but not of zDHHC21, prevented the onset of hippocampus-dependent cognitive deficits and significantly reduced Aβ deposition in 3×Tg-AD female mice (Fig. 4 *C* and *F*). Inhibition of BACE1 S-palmitoylation has been reported to attenuate memory deficits in 5XFAD mice (18). Accordingly, we found that hippocampal knock-down of zDHHC7 reduced BACE1 S-palmitoylation levels in 3×Tg-AD (Fig. 4*E*). However, it is reasonable to hypothesize that the effects on synaptic plasticity and memory observed upon either pharmacological or genetic approaches targeting S-palmitoylation levels were not the result of BACE1 S-palmitoylation reduction only. We found multiple S-palmitoylated targets regulating brain plasticity and survival, and differentially modulated by both 2-BP treatment and zDHHC7 silencing. In addition, dynamic protein S-palmitoylation has been demonstrated to modulate neuronal development and brain plasticity by a plethora of synaptic proteins and signaling pathways (7, 43). Notably, in post-mortem hippocampi of AD patients we found a statistically significant but opposite correlation between BACE1 S-palmitoylation and Aβ 1 to 42 levels (positive correlation) and between BACE1 S-palmitoylation and MMSE score (negative correlation). This evidence, together with the beneficial effects of either pharmacological or genetic inhibition of protein S-palmitoylation on AD-related phenotype, highlights the role of aberrant S-palmitoylation as potential mechanism involved in the onset and progression of AD-related cognitive decline. Nonetheless, some unanswered questions remain. For instance, why and how zDHHC levels increase in AD. We previously demonstrated that BIR induced a FoxO-mediated epigenetic overexpression of zDHHC3 in an experimental model of insulin resistance-dependent cognitive impairment (4). The molecular crosstalk between alteration of insulin signaling and neurodegeneration has been extensively investigated, so that AD has also been named type III diabetes (44–46). We found molecular hallmarks of BIR in the hippocampus of 3×Tg-AD mice at early stages of disease (Fig. 5*A*). Alteration of IRS1-AKT signaling led to inhibition of the transcription factor FoxO1 binding on and epigenetic activation of regulatory sequences of zDHHC7 (Fig. 5*B*). Aβ has been reported to impinge on insulin receptor degradation and to worse insulin signaling in brain areas damaged by neurodegeneration (47). Moreover, FoxO1 expression has been reported to be inversely related to Aβ production in vitro through the transcriptional regulation of BACE1 and Presenilin1 expression (48). It can be hypothesized a sort of vicious circle where, on the one hand alteration of brain insulin signaling, neuroinflammation, and activation of stress-related pathways trigger Aβ production and, on the other hand, Aβ oligomers and oxidative stress

impinge on synaptic function by a plethora of mechanisms including dysregulation of zDHHC expression and protein S-palmitoylation (16, 49, 50). Therefore, zDHHC overexpression would be the result of an abnormal response to different stress.

Our data reveal a key role of zDHHC enzymes in the development of neurodegeneration and cognitive deficits, and suggest that counteracting aberrant protein S-palmitoylation can be an additional therapeutic strategy for AD. We did not detect any change of zDHHC7 or zDHHC21 in the parahippocampal cortex of 3×Tg-AD mice. In addition, zDHHC7 downregulation did not change cognitive function in WT mice nor zDHHC21 silencing did exert beneficial effects on AD phenotype despite its expression was upregulated in the hippocampus of 3×Tg-AD mice. Considering that the hippocampus is one of the most insulin-sensitive brain areas, we hypothesize that the aberrant regulation of zDHHC enzymes may occur later in other brain regions. Moreover, zDHHC enzymes show different levels of expression in different brain areas, they share overlapping substrates, and their activity may be regulated at post-translational level (51, 52). A recent study revealed the critical role of aberrant S-palmitoylation induced by zDHHC21 in the pathophysiology of AD and identified novel mutations in zDHHC21 gene that enhanced S-palmitoylation in a family affected by familiar AD (53). However, we cannot exclude that other S-acyltransferase enzymes may be involved in the onset and progression of neurodegeneration and future studies should investigate the role of all zDHHCs. We also found age-dependent modifications of the expression of several zDHHC enzymes (i.e., 3, 4.5, 15) in the hippocampus of WT mice suggesting that different patterns of zDHHCs and S-palmitoylated proteins may occur across the aging. To date no therapeutic interventions targeting protein S-palmitoylation or zDHHCs have been attempted in AD. Thus, our findings add a layer to the understanding of AD pathophysiology and identify potential therapeutic targets. Given the ever-faster development of drugs inhibiting zDHHC enzymes (e.g., N-cyanomethyl-N-myracrylamide) (54), our results may pave the way for future clinical trials, representing a significant step forward in the field of AD research and to discover effective treatments for neurodegenerative disorders.

Data, Materials, and Software Availability. All study data are included in the article and/or *SI Appendix*.

ACKNOWLEDGMENTS. Fig. 2*A* was created with BioRender.com (2023). We would like to acknowledge the contribution of Electrophysiology and Microscopy Core Facilities Gemelli Science and Technology Park of Fondazione Policlinico Universitario “A. Gemelli” Istituto di Ricovero e Cura a Carattere Scientifico (IRCCS). We would also thank the South West Dementia Brain Bank (SWDBB) and MRC London Brain Bank for Neurodegenerative disease for providing brain tissues for this study. The SWDBB is part of the Brains for Dementia Research program, jointly funded by Alzheimer’s Research United Kingdom (UK) and Alzheimer’s Society and is supported by Bristol Research into Alzheimer’s and Care of the Elderly and the Medical Research Council. The provision of data used in this study was provided with support from the Brains for Dementia Research programme, jointly funded by Alzheimer’s Society UK and Alzheimer’s Society. This research was supported by Cariplo Foundation (Cariplo Telethon Joint Call-GJC21136), Ministero della Università e della Ricerca (PRIN 2022-2022KP5LKS) and Ministero della Salute-Ricerca Corrente 2024 Fondazione Policlinico Universitario A. Gemelli IRCCS.

Author affiliations: ^aDepartment of Neuroscience, Università Cattolica del Sacro Cuore, Rome 00168, Italy; ^bFondazione Policlinico Universitario A. Gemelli, Istituto di Ricovero e Cura a Carattere Scientifico (IRCCS), Rome 00168, Italy; ^cDepartment of Biomedical and Biotechnological Sciences, University of Catania, Catania 95131, Italy; and ^dOasi Research Institute-Istituto di Ricovero e Cura a Carattere Scientifico (IRCCS), Troina 94018, Italy

1. J. F. Dartigues, Alzheimer's disease: A global challenge for the 21st century. *Lancet Neurol.* **8**, 1082–1083 (2009), 10.1016/S1474-4422(09)70298-4.
2. J. Hardy, D. J. Selkoe, The amyloid hypothesis of Alzheimer's disease: Progress and problems on the road to therapeutics. *Science* **297**, 353 (2002).
3. M. Spinelli, S. Fusco, C. Grassi, Brain insulin resistance and hippocampal plasticity: Mechanisms and biomarkers of cognitive decline. *Front. Neurosci.* **13**, 788 (2019), 10.3389/fnins.2019.00788.
4. M. Spinelli *et al.*, Brain insulin resistance impairs hippocampal synaptic plasticity and memory by increasing GluA1 palmitoylation through FoxO3a. *Nat. Commun.* **8**, 2009 (2017), 10.1038/s41467-017-02221-9.
5. J. E. Smotrys, M. E. Linder, Palmitoylation of intracellular signaling proteins: Regulation and function. *Annu. Rev. Biochem.* **73**, 559–587 (2004), 10.1146/annurev.biochem.73.011303.073954.
6. T. Iwanaga *et al.*, Dynamic protein palmitoylation in cellular signaling. *Prog. Lipid Res.* **48**, 117–127 (2009), 10.1016/j.plipres.2009.02.001.
7. Y. Fukata, M. Fukata, Protein palmitoylation in neuronal development and synaptic plasticity. *Nat. Rev. Neurosci.* **11**, 161–175 (2010), 10.1038/nrn2788.
8. R. Bhattacharyya *et al.*, Palmitoylation of amyloid precursor protein regulates amyloidogenic processing in lipid rafts. *J. Neurosci.* **33**, 11169–11183 (2013), 10.1523/JNEUROSCI.4704-12.2013.
9. K. S. Vetrivel *et al.*, Alzheimer disease A β production in the absence of S-palmitoylation-dependent targeting of BACE1 to lipid rafts. *J. Biol. Chem.* **284**, 3793–3803 (2009), 10.1074/jbc.M808920200.
10. E. Cho, M. Park, Palmitoylation in Alzheimer's disease and other neurodegenerative diseases. *Pharmacol. Res.* **111**, 133–151 (2016), 10.1016/j.phrs.2016.06.008.
11. J. Greaves *et al.*, Palmitoylation-induced aggregation of cysteine-string protein mutants that cause neuronal ceroid lipofuscinosis. *J. Biol. Chem.* **287**, 37330–37339 (2012), 10.1074/jbc.M112.389098.
12. F. Natale *et al.*, Neural stem cell-derived extracellular vesicles counteract insulin resistance-induced senescence of neurogenic niche. *Stem Cells* **40**, 318–331 (2022), 10.1093/stmcls/sxab026.
13. S. Fusco *et al.*, Maternal insulin resistance multigenerationally impairs synaptic plasticity and memory via gametic mechanisms. *Nat. Commun.* **10**, 4799 (2019), 10.1038/s41467-019-12793-3.
14. M. Spinelli *et al.*, Neural stem cell-derived exosomes revert HFD-dependent memory impairment via CREB-BDNF signalling. *Int. J. Mol. Sci.* **21**, 8994 (2020), 10.3390/ijms21238994.
15. S. Akkerman *et al.*, Object recognition testing: Statistical considerations. *Behav. Brain Res.* **232**, 317–322 (2012), 10.1016/j.bbr.2012.03.024.
16. T. Guo *et al.*, Molecular and cellular mechanisms underlying the pathogenesis of Alzheimer's disease. *Mol. Neurodegener.* **15**, 40 (2020), 10.1186/s13024-020-00391-7.
17. F. Di Domenico, C. Lanzillotta, The disturbance of protein synthesis/degradation homeostasis is a common trait of age-related neurodegenerative disorders. *Adv. Protein Chem. Struct. Biol.* **132**, 49–87 (2022).
18. R. J. Andrew *et al.*, Lack of BACE1 S-palmitoylation reduces amyloid burden and mitigates memory deficits in transgenic mouse models of Alzheimer's disease. *Proc. Natl. Acad. Sci. U.S.A.* **114**, E9665–E9674 (2017), 10.1073/pnas.1708568114.
19. R. Bhattacharyya *et al.*, Axonal generation of amyloid- β from palmitoylated APP in mitochondria-associated endoplasmic reticulum membranes. *Cell Rep.* **35**, 109134 (2021), 10.1016/j.celrep.2021.109134.
20. J. España *et al.*, Intraneuronal beta-amyloid accumulation in the amygdala enhances fear and anxiety in Alzheimer's disease transgenic mice. *Biol. Psychiatry* **67**, 513–521 (2010), 10.1016/j.biopsych.2009.06.015.
21. R. Sterniczuk, M. C. Antle, F. M. Laferla, R. H. Dyck, Characterization of the 3xTg-AD mouse model of Alzheimer's disease: Part 2. Behavioral and cognitive changes. *Brain Res.* **1348**, 149–155 (2010), 10.1016/j.brainres.2010.06.011.
22. A. E. Kane *et al.*, Sex differences in healthspan predict lifespan in the 3xTg-AD mouse model of Alzheimer's disease. *Front. Aging Neurosci.* **10**, 172 (2018), 10.3389/fnagi.2018.00172.
23. S. Oddo, A. Caccamo, M. Kitazawa, B. P. Tseng, F. M. LaFerla, Amyloid deposition precedes tangle formation in a triple transgenic model of Alzheimer's disease. *Neurobiol. Aging* **24**, 1063–1070 (2003), 10.1016/j.neurobiolaging.2003.08.012.
24. B. Ji, M. Skup, Roles of palmitoylation in structural long-term synaptic plasticity. *Mol. Brain* **14**, 8 (2021), 10.1186/s13041-020-00717-y.
25. L. Matt, K. Kim, D. Chowdhury, J. W. Hell, Role of palmitoylation of postsynaptic proteins in promoting synaptic plasticity. *Front. Mol. Neurosci.* **12**, 8 (2019), 10.3389/fnmol.2019.00008.
26. A. K. Globa, S. X. Bamji, Protein palmitoylation in the development and plasticity of neuronal connections. *Curr. Opin. Neurobiol.* **45**, 210–220 (2017), 10.1016/j.conb.2017.02.016.
27. V. Sposato *et al.*, The medial septum is insulin resistant in the AD presymptomatic phase: Rescue by nerve growth factor-driven IRS1 activation. *Mol. Neurobiol.* **56**, 535–552 (2019), 10.1007/s12035-018-1038-4.
28. A. Tramutola *et al.*, Alteration of mTOR signaling occurs early in the progression of Alzheimer disease (AD): Analysis of brain from subjects with pre-clinical AD, amnesic mild cognitive impairment and late-stage AD. *J. Neurochem.* **133**, 739–749 (2015), 10.1111/jnc.13037.
29. L. L. Beason-Held *et al.*, Health conditions associated with Alzheimer's disease and vascular dementia. *Ann. Neurol.* **93**, 805–818 (2023), 10.1002/ana.26584.
30. J. Pleen, R. Townley, Alzheimer's disease clinical trial update 2019–2021. *J. Neurol.* **269**, 1038–1051 (2022), 10.1007/s00415-021-10790-5.
31. S. A. Tatulin, Challenges and hopes for Alzheimer's disease. *Drug Discov. Today* **27**, 1027–1043 (2022), 10.1016/j.drudis.2022.01.016.
32. C. Hetz, S. Saxena, ER stress and the unfolded protein response in neurodegeneration. *Nat. Rev. Neurosci.* **13**, 477–491 (2017), 10.1038/nrn2017.99.
33. S. Marcelli *et al.*, The involvement of post-translational modifications in Alzheimer's disease. *Curr. Alzheimer Res.* **15**, 313–335 (2018), 10.2174/1567205014666170505095109.
34. N. Yokoi, M. Fukata, Y. Fukata, Synaptic plasticity regulated by protein-protein interactions and posttranslational modifications. *Int. Rev. Cell Mol. Biol.* **297**, 1–43 (2012), 10.1016/B978-0-12-394308-8.00001-7.
35. A. Didonna, F. Benetti, Post-translational modifications in neurodegeneration. *AIMS Biophys.* **3**, 27–49 (2016), 10.3934/biophy.2016.1.27.
36. R. Kang *et al.*, Neural palmitoyl-proteomics reveals dynamic synaptic palmitoylation. *Nature* **456**, 904–909 (2008), 10.1038/nature07605.
37. X. Meckler *et al.*, Reduced Alzheimer's disease β -amyloid deposition in transgenic mice expressing S-palmitoylation-deficient APH1a and nicastrin. *J. Neurosci.* **30**, 16160–16169 (2010), 10.1523/JNEUROSCI.4436-10.2010.
38. D. Davda *et al.*, Profiling targets of the irreversible palmitoylation inhibitor 2-bromopalmitate. *ACS Chem. Biol.* **8**, 1912–1917 (2013), 10.1021/cb400380s.
39. M. P. Pedro *et al.*, 2-Bromopalmitate reduces protein deacylation by inhibition of acyl-protein thioesterase enzymatic activities. *PLoS One* **8**, e75232 (2013), 10.1371/journal.pone.0075232.
40. Z. B. Dong *et al.*, 2-Bromopalmitate decreases spinal inflammation and attenuates oxaliplatin-induced neuropathic pain via reducing Drp1-mediated mitochondrial dysfunction. *PLoS One* **17**, e0275428 (2022), 10.1371/journal.pone.0275428.
41. J. F. Chase, P. K. Tubbs, Specific inhibition of mitochondrial fatty acid oxidation by 2-bromopalmitate and its coenzyme A and carnitine esters. *Biochem. J.* **129**, 55–65 (1972).
42. R. A. Coleman, P. Rao, R. J. Fogelson, E. S. Bards, 2-bromopalmitoyl-CoA and 2-bromopalmitate: Promiscuous inhibitors of membrane-bound enzymes. *Biochim. Biophys. Acta* **1125**, 203–209 (1992).
43. Y. Fukata *et al.*, Local palmitoylation cycles define activity-regulated postsynaptic subdomains. *J. Cell Biol.* **202**, 145–161 (2013), 10.1083/jcb.201302071.
44. S. E. Arnold *et al.*, Brain insulin resistance in type 2 diabetes and Alzheimer disease: Concepts and conundrums. *Nat. Rev. Neurosci.* **14**, 168–181 (2013), 10.1038/nrn2013.185.
45. D. Kellar, S. Craft, Brain insulin resistance in Alzheimer's disease and related disorders: Mechanisms and therapeutic approaches. *Lancet Neurol.* **19**, 758–766 (2020), 10.1016/S1474-4422(20)30231-3.
46. M. Spinelli, S. Fusco, C. Grassi, Brain insulin resistance impairs hippocampal plasticity. *Vitam Horm.* **114**, 281–306 (2020), 10.1016/bs.vh.2020.04.005.
47. C. C. Gali *et al.*, Amyloid beta impairs insulin signaling by accelerating autophagy-lysosomal degradation of LRP-1 and IR- β in blood-brain barrier endothelial cells in vitro and in 3XTg-AD mice. *Mol. Cell Neurosci.* **99**, 103390 (2019).
48. W. Zhang *et al.*, FoxO1 overexpression reduces A β production and tau phosphorylation in vitro. *Neurosci. Lett.* **738**, 135322 (2020), 10.1016/j.neulet.2020.135322.
49. K. N. Manolopoulos, L. O. Klotz, P. Korsten, S. R. Bornstein, A. Barthel, Linking Alzheimer's disease to insulin resistance: The FoxO response to oxidative stress. *Mol. Psychiatry* **15**, 1046–1052 (2010), 10.1038/mp.2010.17.
50. F. G. De Felice, R. A. Gonçalves, S. T. Ferreira, Impaired insulin signalling and allostatic load in Alzheimer disease. *Nat. Rev. Neurosci.* **23**, 215–230 (2022), 10.1038/s41583-022-00558-9.
51. A. R. Wild *et al.*, Exploring the expression patterns of palmitoylating and de-palmitoylating enzymes in the mouse brain using the curated RNA-seq database BrainPalmSeq. *Elife* **11**, e75804 (2022), 10.7554/eLife.75804.
52. M. I. P. Malgapo, M. E. Linder, Substrate recruitment by zDHHC protein acyltransferases. *Open Biol.* **11**, 210026 (2021), 10.1098/rsob.210026.
53. W. Li *et al.*, Aberrant palmitoylation caused by a ZDHHC21 mutation contributes to pathophysiology of Alzheimer's disease. *BMC Med* **21**, 223 (2023), 10.1186/s12916-023-02930-7.
54. T. Lan, C. Delalande, B. C. Dickinson, Inhibitors of DHH family proteins. *Curr. Opin. Chem. Biol.* **65**, 118–125 (2021), 10.1016/j.cba.2021.07.002.